


 Cite this: *RSC Adv.*, 2019, **9**, 4665

 Received 10th December 2018  
 Accepted 28th January 2019

DOI: 10.1039/c8ra10123j

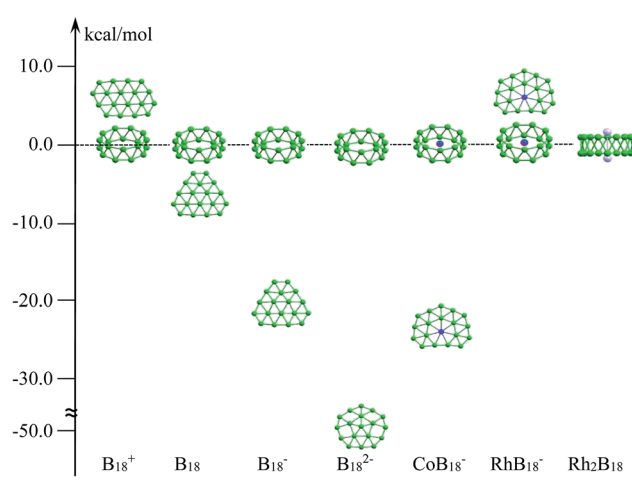
rsc.li/rsc-advances

## 1. Introduction

Zero-dimensional boron clusters have received incessant attention from the aspects of their molecular shapes and multi-center bonding.<sup>1,2</sup> In comparison with cage-like structured bulk boron,<sup>3</sup> boron clusters  $B_n$ , from small size to an extended size range at least up to  $B_{38}^-$  ( $B_{16}^{+}$ ), prefer to form planar or quasi-planar structures, which have been confirmed *via* experimental and high-level computational studies.<sup>4,5</sup> Remarkably, over past decades, a set of pure and doped boron clusters have been systematically characterized, which constantly pushes our current understanding of the structural evolution of isolated boron clusters.<sup>6-8</sup> Recently, the discovery of all-boron fullerenes,<sup>9,10</sup> borophenes and boron sheets on metal surfaces,<sup>11-14</sup> motivated by their carbon analogues, has overwhelmingly enriched studies of the chemistry of boron and may lead to new boron-based materials. On the other hand, studies of doped boron clusters with transition metals, such as metal-centered monocyclic rings,<sup>7</sup> metalloborophenes,<sup>15</sup> half-sandwich structures,<sup>16,17</sup> and metal-centered tubular structures and cages,<sup>18-23</sup> have created a series of clusters with novel structures and chemical bonding. All these doped-boron clusters have pushed the limits of recorded coordination numbers and structural chemistry.

Tubular boron structures are a very special case in terms of isolated boron clusters. They have aroused widespread interest for many years because they can be considered not only as a key indicator of the 2D-to-3D (planar to three-dimensional form)

structural transition of boron clusters, but also as embryos for boron nanotubes. The two-ring  $B_{20}$  tubular cluster is the first example and it is characterized as the global minimum on the basis of computational calculations, yet it has not been observed experimentally.<sup>24,25</sup> Remarkably, cationic  $B_{2n}^+$  ( $n = 9-10$ ) tubular structures were clearly confirmed *via* joint ion mobility experiments combined with density functional theory (DFT) calculations.<sup>5</sup> For anionic boron clusters, planar or quasi-planar boron (2D) forms remain critical competing alternatives that are more stable in energy than the tubular forms; this has been confirmed *via* photoelectron spectroscopy (PES) combined with theoretical investigations.<sup>26-28</sup> The 2D preference of negatively charged boron clusters can be ascribed to the fact that electron addition tends to enhance the stability of the 2D form over the corresponding 3D isomer, irrespective of the available electrons.<sup>29</sup> For instance, as shown in Scheme 1, the tubular



Scheme 1 The relative energy differences in  $\text{kcal mol}^{-1}$  between tubular structures and low-lying planar forms at the DFT level.<sup>5,30-32</sup>

<sup>a</sup>Institute of Atomic and Molecular Physics, Jilin Provincial Key Laboratory of Applied Atomic and Molecular Spectroscopy, Jilin University, Changchun, China. E-mail: [zcui@jlu.edu.cn](mailto:zcui@jlu.edu.cn)

<sup>b</sup>Department of Chemistry, Indian Institute of Engineering Science and Technology, Shibpur, Howrah, India

† Electronic supplementary information (ESI) available. See DOI: [10.1039/c8ra10123j](https://doi.org/10.1039/c8ra10123j)



structure of  $B_{18}^+$  was suggested to be the global minimum, whereas the  $B_{18}^-$ ,  $B_{18}^{2-}$  and  $B_{18}^{3-}$  analogues were found to be high-energy isomers.<sup>5,30-32</sup> Meanwhile, it is noted that the stability of a tubular structure deceases along with an increase in electrons, so it is difficult to stabilize doubly or more negatively charged boron tubular clusters. Interestingly, doped boron clusters with transition metals have led to the achievement of mono-metal-centered tubular boron clusters. Recently, tubular  $MB_{16}^-$  ( $M = Co, Mn$ ),  $RhB_{18}^-$  and  $TaB_{20}^-$  have been characterized *via* PES combined with theoretical predictions.<sup>18,22,33,34</sup> Clearly, the strong covalent interactions between the transition metal and tubular boron motifs significantly stabilize the tubular structures. Recent works have shown that the tubular-to-cage-like structural transition has started in large mono-metal-based boron clusters.<sup>21,35</sup>

Our recent work revealed that the thermodynamic stability of tubular boron clusters was significantly promoted in Li-doped boron species ( $LiB_{20}$  and  $LiB_{20}^-$ ) in comparison with bare anionic  $B_{20}$  species.<sup>36</sup> This is because the optimal electrostatic interactions arising from charge transfer significantly improve the stability of tubular boron clusters. In this work, we followed the same strategy and found that the effects from two doped Na atoms can tune the preference between 2D and tubular forms in the difficult case of negatively charged  $B_{18}$ , where the tubular form is a high-energy isomer. Herein we report an investigation into di-alkali metal doped boron clusters in the form of  $Na_2B_{18}$  and  $Na_2B_{18}^-$  species. Surprisingly, rather than forming a half-sandwich structure with the quasi-planar structure of bare  $B_{18}$ ,  $B_{18}^-$  and  $B_{18}^{2-}$ , the  $Na_2B_{18}$  and  $Na_2B_{18}^-$  clusters are predicted to have tubular structures, where the two Na atoms are located on the high-symmetry axis of the tubular structures and the two sides of the double-ring boron. Chemical bonding analysis has revealed that the tubular clusters are charge-transfer complexes formed by  $Na^+$  and  $B_{18}^{2-}$  ( $B_{18}^{3-}$ ), where the optimal electrostatic interactions between Na and boron clusters are found.

## 2. Computational details

The structure search is performed using the PSO algorithm within the revolutionary scheme, as implemented *via* CALYPSO (Crystal structure AnaLYsis by Particle Swarm Optimization) code.<sup>37</sup> Specifically, in the PSO search, the population size is set to 30, and the number of generations is maintained at 30. The best 60% of structures are selected through PSO to generate the next generation, while the other structures are generated randomly to guarantee structural diversity. The B3LYP/6-31G(d) level of theory was used to optimize the initial structure with a variety of spin states, and for the low-lying (<30 kcal mol<sup>-1</sup> above the global minimum) isomers, we employed B3LYP/6-311+G(d) and TPSSh/6-311+G(d) for better geometrical and frequency predictions. The single-point calculations for the low-lying isomers were performed at the CCSD(T)/6-311+G(d)/TPSSh/6-311+G(d) level of theory. We found that T1 values are in the range of 0.01 to 0.03 for the low-lying isomers, indicating that the mono-determinantal method can be safely employed for our species. Electron detachment energies from the closed-

shell ground state of  $Na_2B_{18}^-$  and the low-lying isomers were computed at the TD-B3LYP/6-311+G(2df) level of theory based on B3LYP/6-311+G(d) geometry. The chemical bonding in  $Na_2B_{18}$  and  $Na_2B_{18}^-$  has been revealed *via* natural bonding orbital (NBO)<sup>38</sup> and adaptive natural density partitioning (AdNDP) algorithm analysis.<sup>39</sup> Total energies were corrected using the zero-point energies (ZPE). All calculations were carried out with the GAUSSIAN09 program package.<sup>40</sup>

## 3. Results and discussion

CALYPSO was performed to explore the potential energy surfaces of neutral  $Na_2B_{18}$  and anionic  $Na_2B_{18}^-$  clusters in low and high spin states. At the B3LYP/6-311+G(d) and TPSSh/6-311+G(d) levels of theory, the tubular structures of  $Na_2B_{18}$  and  $Na_2B_{18}^-$  were found to be local minima, with large lowest frequencies of above 100.0 cm<sup>-1</sup> (see Table 1) and high  $D_{9d}$ -symmetry, where the two Na atoms are located on the high-symmetry axis of the tubular structures (see Fig. 1). Furthermore, the tubular structures were predicted to be global minima at the B3LYP, TPSSh and single-point CCSD(T) levels of theory with the 6-311+G(d) basis set. In particular, they are 2.1 and 2.0 kcal mol<sup>-1</sup> more stable than the second lowest isomers of the  $Na_2B_{18}$  and  $Na_2B_{18}^-$  species, respectively, at the single-point CCSD(T)/6-311+G(d)/TPSSh/6-311+G(d) level of theory. All low-lying isomers are provided in the ESI.† For the nearest competing isomers, the  $B_{18}$  motif possesses a quasi-planar structure that is similar to the low-lying isomers of bare anionic  $B_{18}^{2-}$ , and the two Na atoms were located above or beside the quasi-plane of the boron clusters.

The structural details of the tubular structures of  $Na_2B_{18}$  and  $Na_2B_{18}^-$  are tabulated in Table 1. The structures of the neutral and anionic forms are very similar, except for the significant difference in the Na-B and Na-Na interaction distances. Contrasting with neutral  $Na_2B_{18}$ , the Na-B and Na-Na interaction distances in the  $Na_2B_{18}^-$  cluster were clearly reduced by 0.06 and 0.17 Å, respectively. The calculated natural atomic charge on the Na atom is about 0.95 |e| in the  $Na_2B_{18}$  and  $Na_2B_{18}^-$  species, indicating that Na serves as the donor of one electron to the  $B_{18}$  tubular motifs, forming typical charge-transfer  $Na_2^{2+}B_{18}^{2-}$  and  $Na_2^{2+}B_{18}^{3-}$  complexes. The calculated natural atomic charges on the B atoms are -0.11 and -0.16 |e| in the  $Na_2B_{18}$  and  $Na_2B_{18}^-$  species, respectively, resulting in stronger electrostatic interactions between  $Na^+$  and the anionic boron cluster in the  $Na_2B_{18}^-$  system compared to the neutral analogue. This is the reason that shorter Na-B and Na-Na interaction distances were found in the anionic  $Na_2B_{18}^-$  system. It is worth noting that the Na-B bond distances in both neutral and anionic  $Na_2B_{18}$  are longer than a Na-B single bond (2.4 Å) obtained using the self-consistent covalent radii of Pyykkö,<sup>41</sup> which is consistent with the negligible Wiberg bond indices (WBIs) listed in Table 1. Clearly, the two kinds of B-B bonds, inter-ring and intra-ring, are found in both neutral and anionic tubular species. The inter-ring B-B bonds are responsible for holding two monocyclic  $B_9$  rings together, and are clearly longer (about 0.07 Å) than the intra-ring B-B bonds (1.62 Å). The WBIs of the two kinds of B-B bonds further confirm the assessment of



**Table 1** The smallest frequencies ( $V_{\min}$ ,  $\text{cm}^{-1}$ ) of the tubular structures, NPA charges on Na and B ( $Q_{\text{Na}}$  and  $Q_{\text{B}}$ ,  $|\epsilon|$ ), bond properties (bond length ( $\text{\AA}$ ), Wiberg bond indices in parenthesis) and HOMO–LUMO gaps (gap, eV). All values have been computed at the B3LYP/6-311+G(d) level of theory

Species	$V_{\min}$ ( $\text{cm}^{-1}$ )	$B_{\text{Na-Na}}$ ( $\text{\AA}$ )	$B_{\text{Na-B}}$ ( $\text{\AA}$ )	$B_{\text{B-B}}$ ( $\text{\AA}$ )	$Q_{\text{Na}}$ ( $ \epsilon $ )	$Q_{\text{B}}$ ( $ \epsilon $ )	Gap (eV)
$\text{Na}_2\text{B}_{18}$	131.3	4.501 (0.00)	2.810 (0.01)	1.688; 1.619 (0.71); (0.96)	0.96	-0.11	2.07
$\text{Na}_2\text{B}_{18}^-$	176.1	4.329 (0.00)	2.751 (0.01)	1.713; 1.615 (0.65); (1.01)	0.95	-0.16	1.15

bond distances. Moreover, their strength can be referenced to the value of a typical B–B single bond (1.70  $\text{\AA}$ ). It is worthy of note that two such kinds of B–B bonds have been found in all the tubular structures of pure boron or hetero-doped boron clusters. Note that the formation of Na–B interactions in  $\text{Na}_2\text{B}_{18}$  and  $\text{Na}_2\text{B}_{18}^-$  species effectively removes the electronic charge of two Na atoms, which evidently promotes the electrostatic interactions between  $\text{Na}^+$  and the tubular boron motifs, giving rise to the eighteen optimal Na–B interactions and high thermodynamic stability of the tubular structures.

As discussed above, both  $\text{Na}_2\text{B}_{18}$  and  $\text{Na}_2\text{B}_{18}^-$  species are essentially charge-transfer complexes between  $\text{Na}^+$  and  $\text{B}_{18}^{2-}$  ( $\text{B}_{18}^{3-}$ ). To discover how the further thermodynamic stability of tubular structures is gained, we investigated two kinds of dissociation pathways by means of: (i)  $\text{Na}_2\text{B}_{18} \rightarrow 2\text{Na}^+ + \text{B}_{18}^{2-}$  and (ii)  $\text{Na}_2\text{B}_{18} \rightarrow 2\text{Na} + \text{B}_{18}$ ; and (iii)  $\text{Na}_2\text{B}_{18}^- \rightarrow 2\text{Na}^+ + \text{B}_{18}^{3-}$  and (iv)  $\text{Na}_2\text{B}_{18}^- \rightarrow 2\text{Na} + \text{B}_{18}^-$  for the  $\text{Na}_2\text{B}_{18}$  and  $\text{Na}_2\text{B}_{18}^-$  species, where all these fragments are in their electronic ground states. At the TPSSh/6-311+G(d) level of theory, pathways (i) and (ii) for  $\text{Na}_2\text{B}_{18}$  give dissociation energies of 283.1 and 121.7 kcal  $\text{mol}^{-1}$ , respectively, and pathways (iii) and (iv) for  $\text{Na}_2\text{B}_{18}^-$  give dissociation energies of 441.4 and 81.5 kcal  $\text{mol}^{-1}$ , respectively. The high dissociation energies indicate the good stability against the dissociation of M and  $\text{M}^+$  for tubular motifs. Additionally, the degrees of  $\text{Na}^+$  and tubular boron interaction could be approximately estimated and compared. The interaction energies between  $\text{Na}^+$  and tubular boron are estimated to be 171.5 and 253.9 kcal  $\text{mol}^{-1}$ , half of the total dissociation energies of pathways (i) and (iii), respectively, where the boron fragments are in ground electronic states with

the framework of a tubular structure. Strong electrostatic interactions between  $\text{Na}^+$  and the tubular boron motifs provide a key driving force for stabilizing these charge-transfer complexes in the neutral and anionic states. The optimized structures of the bare tubular  $\text{B}_{18}^{2-}$  and  $\text{B}_{18}^{3-}$  clusters lie 59.8 and 64.3 kcal  $\text{mol}^{-1}$  higher in energy, respectively, than the quasi-planar minimum at the TPSSh/6-311+G(d) level of theory. The tubular structures of the anionic  $\text{B}_{18}^{2-}$  and  $\text{B}_{18}^{3-}$  species are significantly stabilized by means of doping two cationic  $\text{Na}^+$  ions, resulting in effective charge transfer in the tubular structures. Moreover, additional electrostatic stabilization occurred in  $\text{Na}_2\text{B}_{18}^-$  compared to  $\text{Na}_2\text{B}_{18}$  via one more electron being only localized in the tubular boron motifs. Thus, only electrostatic interactions between Na and the  $\text{B}_{18}$  clusters make  $\text{Na}_2\text{B}_{18}$  and  $\text{Na}_2\text{B}_{18}^-$  highly thermodynamically stable species.

The molecular orbitals of  $\text{Na}_2\text{B}_{18}^-$  are given in Fig. S2,† and one unpaired electron resides in a singly occupied molecular orbital (SOMO) instead of a closed-shell neutral one. To further understand the structure and stability of the tubular structure, we analyzed the chemical bonding of the  $\text{Na}_2\text{B}_{18}$  system using the adaptive natural density partitioning (AdNDP) method at the B3LYP/6-311+G(d) level of theory. AdNDP analysis transformed the 28 canonical molecular orbitals of the  $\text{Na}_2\text{B}_{18}$  system into localized and delocalized multi-center bonds, as shown in Fig. 2. There are three types of bond in the tubular boron cluster. The first row depicts eighteen two center-two electron (2c–2e) localized  $\sigma$  bonds with an occupation number (ON) of 1.85  $|\epsilon|$ , which is very similar to the ON of a bare  $\text{B}_{18}$  cluster, as shown in the ESI.† The remaining AdNDP bonds can be considered as delocalized multi-center  $\sigma$  and  $\pi$  bonds

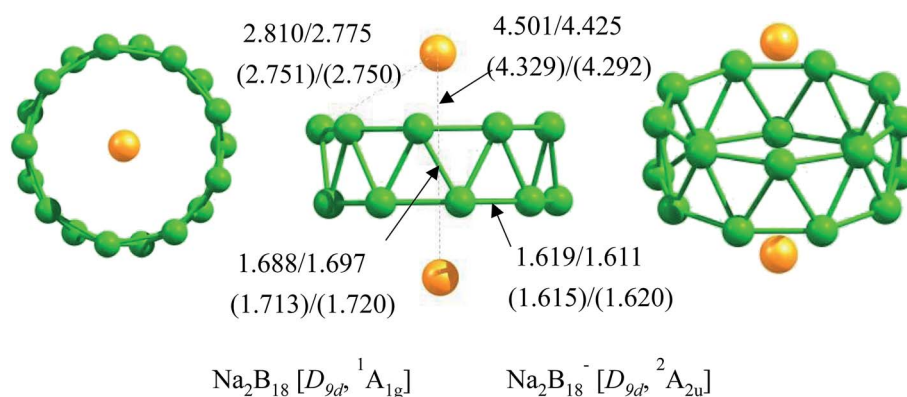


**Fig. 1** Three views of the  $\text{Na}_2\text{B}_{18}$  and  $\text{Na}_2\text{B}_{18}^-$  species. The point group symmetries and spectroscopic states are shown in square brackets. All distances are in  $\text{\AA}$ ; the values shown in parentheses refer to the anionic  $\text{Na}_2\text{B}_{18}^-$  system, the values before the backslash are obtained at the B3LYP/6-311+G(d) level of theory and the ones after the backslash are obtained at the TPSSh/6-311+G(d) level of theory.



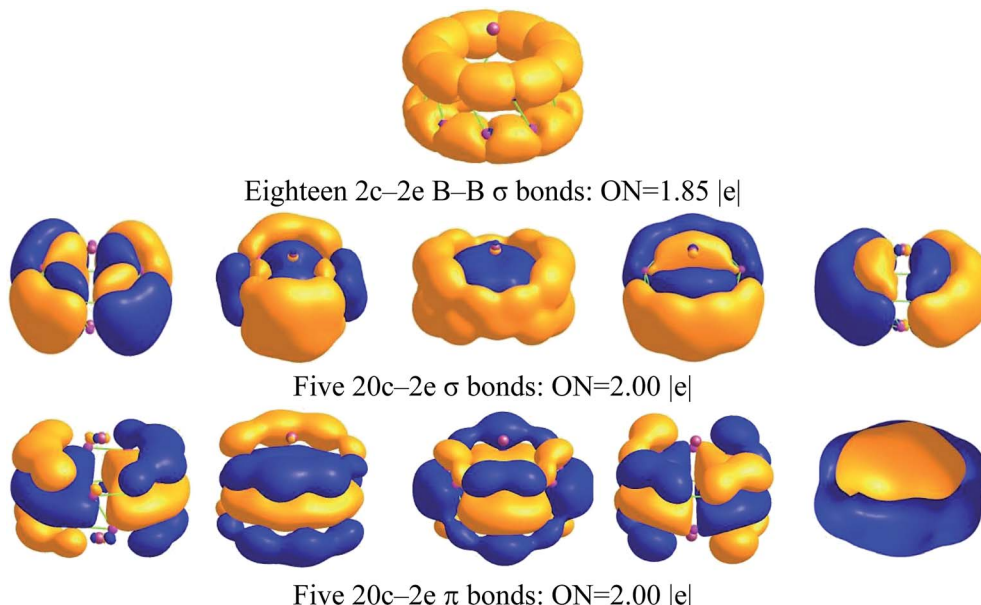


Fig. 2 AdNDP analysis of  $\text{Na}_2\text{B}_{18}$  computed at the B3LYP/6-311+G(d) level of theory; ON stands for occupation number.

between the two  $\text{B}_9$  rings. The second and third rows exhibit five delocalized  $\sigma$  and  $\pi$  bonds, respectively, representing strong bonding interactions between the five delocalized  $\sigma$  and  $\pi$  bonds in each  $\text{B}_9$  ring. The second and third row each describe an aromatic system, resulting in fairly stable  $D_{9d}$  tubular  $\text{Na}_2\text{B}_{18}$  clusters.

To facilitate the future experimental characterization of the anionic tubular  $\text{Na}_2\text{B}_{18}^-$  system, we use time-dependent (TD)-B3LYP/6-311+G(2df) theory to calculate the vertical electron detachment energies (VDEs) for the three lowest energy isomers. Tubular  $\text{Na}_2\text{B}_{18}^-$  is predicted to have an extremely low first VDE of 1.65 eV, originating from the detachment of the electron from the SOMO, which is significantly lower in energy than the other low-lying isomers by about 0.9 eV (see Table S1–S3†). The first adiabatic electron detachment energy (ADE) is calculated as the total energy difference between  $\text{Na}_2\text{B}_{18}^-$  and  $\text{Na}_2\text{B}_{18}$  using their respective optimized geometries. The ADE values are 1.63, 1.97 and 1.88 eV for the three low-lying isomers I, II and III. Overall, the tubular structure has a clear signal compared to the other low-lying isomers and this can be distinguished in experiments. The calculated infrared (IR) absorption spectrum of the neutral  $\text{Na}_2\text{B}_{18}$  tubular structure is depicted in Fig. S5,† which should aid the forthcoming experimental characterization of the tubular structures.

Small boron clusters have been found to show planar and quasi-planar preferences and electron delocalization in both the  $\sigma$  and  $\pi$  frameworks has been shown to be the major driving force. A tubular structure was first shown to be viable for the neutral  $\text{B}_{20}$  cluster and was suggested to be the embryo for boron nanotubes.<sup>24</sup> Ion mobility and DFT calculations suggested that cationic boron clusters ( $\text{B}_n^+$ ) prefer to take up tubular structures for  $n > 15$ .<sup>5</sup> However, for anionic  $\text{B}_n^-$  clusters, no tubular clusters have been observed up to  $n = 40$ .<sup>4</sup> This trend results from the fact that electron addition tends to enhance the

stability of 2D isomers over the corresponding 3D isomers, irrespective of the available electrons. Clearly, the strong metal–boron covalent interactions in  $\text{CoB}_{16}^-$ ,  $\text{MnB}_{16}^-$  and  $\text{RhB}_{18}^-$  are critical in stabilizing tubular structures, and they require a perfect electronic and structural match between the metal and the boron cluster to justify the balance between M–B interactions in the tubular isomers and 2D electron delocalization.<sup>18,33,34</sup> By means of a detailed analysis of the structural and electronic properties, the anionic tubular structures stabilized by doped alkali metals are found to be due to strong electrostatic interactions between  $\text{Na}^+$  and the anionic  $\text{B}_{18}$  motifs. Following this idea, we further extend this strategy to the other alkali metals ( $\text{M} = \text{Li}, \text{K}$ ). The initial geometries were constructed by replacing Na with M atoms in term of the isomers of the Na-doped system, as shown in Fig. S1 and S2.† As shown in Fig. S6,† all the low-lying isomers are given for the  $\text{M}_2\text{B}_{18}$  and  $\text{M}_2\text{B}_{18}^-$  ( $\text{M} = \text{Li}, \text{K}$ ) species. As predicted, the tubular boron clusters were the lowest-energy isomers for all species at the TPSSh/6-311+G(d) level of theory. In the case of tubular boron structures, two kinds of B–B bond show an insignificant change for all the M-doped systems ( $\text{M} = \text{Li}, \text{Na}, \text{K}$ ), whereas the M–B and M–M interaction distances increase along with the size of the alkali metal (see Fig. S7†). This work suggests a new strategy where the electrostatic interactions can be used to clearly tune the boron arrangement preference, which is further useful for understanding the structural evolution of boron clusters.

## 4. Conclusions

In summary, we present a symmetric theoretical investigation into the viability of tubular structures in  $\text{Na}_2\text{B}_{18}$  and  $\text{Na}_2\text{B}_{18}^-$  clusters. We found that tubular structures with high  $D_{9d}$  symmetry have been predicted to be global minima *via* high-level calculations. Chemical bonding analysis revealed that

the tubular structures are charge-transfer complexes, where the two Na atoms are localized on the axis of the tubular structure, giving rise to optimal Na–B electrostatic interactions. The strong electrostatic interactions between  $\text{Na}^+$  atoms and tubular boron structures appear to be critical in stabilizing the tubular structure, which is an unfavorable configuration in comparison to the quasi-planar and planar arrangement of pure anionic boron species because of 2D electron delocalization. The  $\text{Na}_2\text{B}_{18}$  and  $\text{Na}_2\text{B}_{18}^-$  species represent a new class of metal-doped boron clusters, providing new insights into tubular boron species and further recommending boron clusters as a promising building block for new boron-based nanostructures.

## Conflicts of interest

There are no conflicts to declare.

## Acknowledgements

This work was funded by the National Natural Science Foundation of China (No. 11874178, 21503088). Anita Das acknowledges SERB, India, for providing a National Post-Doctoral Fellowship (N-PDF application no. PDF/2017/000315). The partial calculations in this work were supported by the High Performance Computing Center of Jilin University, China.

## References

- 1 T. Kondo, *Sci. Technol. Adv. Mater.*, 2017, **18**, 780–804.
- 2 L.-S. Wang, *Int. Rev. Phys. Chem.*, 2016, **35**, 69–142.
- 3 A. R. Oganov, J. Chen, C. Gatti, Y. Ma, Y. Ma, C. W. Glass, Z. Liu, T. Yu, O. O. Kurakevych and V. L. Solozhenko, *Nature*, 2009, **457**, 863–867.
- 4 W.-L. Li, X. Chen, T. Jian, T.-T. Chen, J. Li and L.-S. Wang, *Nat. Rev. Chem.*, 2017, **1**, 71.
- 5 E. Oger, N. R. M. Crawford, R. Kelting, P. Weis, M. M. Kappes and R. Ahlrichs, *Angew. Chem., Int. Ed.*, 2007, **46**, 8503–8506.
- 6 A. P. Sergeeva, I. A. Popov, Z. A. Piazza, W.-L. Li, C. Romanescu, L.-S. Wang and A. I. Boldyrev, *Acc. Chem. Res.*, 2014, **47**, 1349–1358.
- 7 C. Romanescu, T. R. Galeev, W.-L. Li, A. I. Boldyrev and L.-S. Wang, *Acc. Chem. Res.*, 2013, **46**, 350–358.
- 8 A. N. Alexandrova, A. I. Boldyrev, H. J. Zhai and L. S. Wang, *Coord. Chem. Rev.*, 2006, **250**, 2811–2866.
- 9 H.-J. Zhai, Y.-F. Zhao, W.-L. Li, Q. Chen, H. Bai, H.-S. Hu, Z. A. Piazza, W.-J. Tian, H.-G. Lu, Y.-B. Wu, Y.-W. Mu, G.-F. Wei, Z.-P. Liu, J. Li, S.-D. Li and L.-S. Wang, *Nat. Chem.*, 2014, **6**, 727–731.
- 10 J. Lv, Y. Wang, L. Zhu and Y. Ma, *Nanoscale*, 2014, **6**, 11692–11696.
- 11 W. L. Li, Q. Chen, W. J. Tian, H. Bai, Y. F. Zhao, H. S. Hu, J. Li, H. J. Zhai, S. D. Li and L. S. Wang, *J. Am. Chem. Soc.*, 2014, **136**, 12257–12260.
- 12 A. J. Mannix, X.-F. Zhou, B. Kiraly, J. D. Wood, D. Alducin, B. D. Myers, X. Liu, B. L. Fisher, U. Santiago, J. R. Guest, M. J. Yacaman, A. Ponce, A. R. Oganov, M. C. Hersam and N. P. Guisinger, *Science*, 2015, **350**, 1513–1516.
- 13 B. Feng, J. Zhang, Q. Zhong, W. Li, S. Li, H. Li, P. Cheng, S. Meng, L. Chen and K. Wu, *Nat. Chem.*, 2016, **8**, 563–568.
- 14 Z. Zhang, Y. Yang, E. S. Penev and B. I. Yakobson, *Adv. Funct. Mater.*, 2017, **27**, 1605059.
- 15 W.-L. Li, T. Jian, X. Chen, T.-T. Chen, G. V. Lopez, J. Li and L.-S. Wang, *Angew. Chem., Int. Ed.*, 2016, **55**, 7358–7363.
- 16 T.-T. Chen, W.-L. Li, T. Jian, X. Chen, J. Li and L.-S. Wang, *Angew. Chem., Int. Ed.*, 2017, **56**, 6916–6920.
- 17 I. A. Popov, W. Li, Z. A. Piazza, A. I. Boldyrev and L. Wang, *J. Phys. Chem. A*, 2014, **118**, 8098–8105.
- 18 I. a Popov, T. Jian, G. V Lopez, A. I. Boldyrev and L.-S. Wang, *Nat. Commun.*, 2015, **6**, 8654.
- 19 J. Lv, Y. Wang, L. Zhang, H. Lin, J. Zhao and Y. Ma, *Nanoscale*, 2015, **7**, 10482–10489.
- 20 N. M. Tam, H. T. Pham, L. Van Duong, M. P. Pham-Ho and M. T. Nguyen, *Phys. Chem. Chem. Phys.*, 2015, **17**, 3000–3003.
- 21 H.-R. Li, H. Liu, X.-X. Tian, W.-Y. Zan, Y.-W. Mu, H.-G. Lu, J. Li, Y.-K. Wang and S.-D. Li, *Phys. Chem. Chem. Phys.*, 2017, **19**, 27025–27030.
- 22 W.-L. Li, T. Jian, X. Chen, H.-R. Li, T.-T. Chen, X.-M. Luo, S.-D. Li, J. Li and L.-S. Wang, *Chem. Commun.*, 2017, **53**, 1587–1590.
- 23 Y. Wang, X. Wu and J. Zhao, *J. Cluster Sci.*, 2018, **29**, 847–852.
- 24 B. Kiran, S. Bulusu, H.-J. Zhai, S. Yoo, X. C. Zeng and L.-S. Wang, *Proc. Natl. Acad. Sci. U. S. A.*, 2005, **102**, 961–964.
- 25 C. Romanescu, D. J. Harding, A. Fielicke and L.-S. Wang, *J. Chem. Phys.*, 2012, **137**, 14317.
- 26 A. P. Sergeeva, Z. A. Piazza, C. Romanescu, W. L. Li, A. I. Boldyrev and L. S. Wang, *J. Am. Chem. Soc.*, 2012, **134**, 18065–18073.
- 27 I. A. Popov, Z. A. Piazza, W.-L. Li, L.-S. Wang and A. I. Boldyrev, *J. Chem. Phys.*, 2013, **139**, 144307.
- 28 X.-M. Luo, T. Jian, L.-J. Cheng, W.-L. Li, Q. Chen, R. Li, H.-J. Zhai, S.-D. Li, A. I. Boldyrev, J. Li and L.-S. Wang, *Chem. Phys. Lett.*, 2017, **683**, 336–341.
- 29 H. T. Pham, L. Van Duong, B. Q. Pham and M. T. Nguyen, *Chem. Phys. Lett.*, 2013, **577**, 32–37.
- 30 A. P. Sergeeva, B. B. Averkiev, H.-J. Zhai, A. I. Boldyrev and L.-S. Wang, *J. Chem. Phys.*, 2011, **134**, 224304.
- 31 D. Moreno, S. Pan, L. L. Zeonjuk, R. Islas, E. Osorio, G. Martínez-Guajardo, P. K. Chattaraj, T. Heine and G. Merino, *Chem. Commun.*, 2014, **50**, 8140–8143.
- 32 T. B. Tai, N. M. Tam and M. T. Nguyen, *Chem. Phys. Lett.*, 2012, **530**, 71–76.
- 33 T. Jian, W.-L. Li, I. A. Popov, G. V. Lopez, X. Chen, A. I. Boldyrev, J. Li and L.-S. Wang, *J. Chem. Phys.*, 2016, **144**, 154310.
- 34 T. Jian, W.-L. Li, X. Chen, T.-T. Chen, G. V. Lopez, J. Li and L.-S. Wang, *Chem. Sci.*, 2016, **7**, 7020–7027.
- 35 H.-R. Li, H. Liu, X.-Q. Lu, W.-Y. Zan, X.-X. Tian, H.-G. Lu, Y.-B. Wu, Y.-W. Mu and S.-D. Li, *Nanoscale*, 2018, **10**, 7451–7456.
- 36 W. Liang, A. Das, X. Dong and Z. Cui, *Phys. Chem. Chem. Phys.*, 2018, **20**, 16202–16208.
- 37 H. Wang, Y. Wang, J. Lv, Q. Li, L. Zhang and Y. Ma, *Comput. Mater. Sci.*, 2016, **112**, 406–415.



38 A. E. Reed, R. B. Weinstock and F. Weinhold, *J. Chem. Phys.*, 1985, **83**, 735–746.

39 D. Y. Zubarev and A. I. Boldyrev, *Phys. Chem. Chem. Phys.*, 2008, **10**, 5207–5217.

40 M. J. Frisch, G. W. Trucks, H. B. Schlegel, G. E. Scuseria, M. A. Robb, J. R. Cheeseman, G. Scalmani, V. Barone, B. Mennucci, G. A. Petersson, *et al.*, *Gaussian 09, Revision D.01*, Gaussian, Inc., Wallingford, CT, 2009.

41 P. Pyykko and M. Atsumi, *Chem.-Eur. J.*, 2009, **15**, 12770–12779.

